Available online at www.sciencedirect.com
ScienceDirect
Journal of Sound and Vibration 304 (2007) 587–605
JOURNAL OF SOUND AND VIBRATION
www.elsevier.com/locate/jsvi

Discrete Huygens' modeling for the characterization of a sound absorbing medium

L. Chai[a,*], Y. Kagawa[b]

[a]*Graduate School of Engineering Nuclear Power & Energy, Safety Engineering Course, University of Fukui, 3-931 Bunkyo, Fukui City, Fukui Prefecture 910-8507, Japan*
[b]*Department of Electrical and Electronic Engineering, College of Industrial Technology, Nihon University, Japan*

Received 31 March 2006; received in revised form 7 December 2006; accepted 3 March 2007
Available online 26 April 2007

Abstract

Based on the equivalence between the wave propagation in the electrical transmission-lines and acoustic tubes, the authors proposed the use of the transmission-line matrix modeling (TLM) for time-domain solution method of the sound field. TLM is known in electromagnetic engineering community, which is equivalent to the discrete Huygens' modeling. The wave propagation is simulated by tracing the sequences of the transmission and scattering of impulses. The theory and the demonstrated examples are presented in the references, in which a sound absorbing field was preliminarily considered to be a medium with simple acoustic resistance independent of frequency and the angle of incidence for the absorbing layer placed on the room wall surface. The present work is concerned with the time-domain response for the characterization of the sound absorbing materials. A lossy component with variable propagation velocity is introduced for sound absorbing materials to facilitate the energy consumption. The frequency characteristics of the absorption coefficient are also considered for the normal, oblique and random incidence. Some numerical demonstrations show that the present modeling provide a reasonable modeling of the homogeneous sound absorbing materials in time domain.

1. Introduction

Time domain analysis or transient response analysis is becoming more and more important as the increase of the capability of the digital computers. It is more realistic and provides full wave analysis. Electro-acoustical engineers have been favored the use of the electrical circuit analogy to acoustical problems. This dynamical analogy has extensively been used for the acoustical device design [1–4]. This is because many of the engineers involving with the electro-acoustical device design are electrical engineers and the electrical components are well established under long wave-length assumption. Their counterparts have been introduced in mechanical and acoustical systems. As in electro-mechanical-acoustical devices electrical, mechanical and acoustical systems are coupled, the unified approach is not only convenient but also provides a model, which

*Corresponding author.
E-mail address: chaily123@yahoo.co.jp (L. Chai).

0022-460X/$ - see front matter © 2007 Elsevier Ltd. All rights reserved.
doi:10.1016/j.jsv.2007.03.001

helps the over-view and the understanding of their physical behaviors. It is possible to solve the problems completely numerically. That is, the differential equations established are numerically solved, in which the response is simply obtained for a certain input. The system in consideration is a block box in which its physical insight is lost. Engineers are those who like to have an intuitive understanding.

Craggs proposed the sound absorbing materials based on the finite element modeling in frequency domain [5,6]. One of the present authors proposed a finite-element equivalent circuits for acoustical field [7]. They are all modeled for frequency domain. With the advent of the digital signal processing, the time domain modeling is frequently required. It is not only reflecting the real problem but also gives full wave analysis. The tracing of the applied and reflected impulses forms the discrete time signals which match the digital signal processing. In fact, the field discretized is interpreted as a series of the connections of digital filters.

Based on the equivalence between the wave propagation in the electrical transmission-lines and acoustic tubes, the authors proposed the use of the transmission-line matrix modeling (TLM) for simulating the sound field in time-domain, which is well-known in electromagnetic engineering community [8]. The propagation is simulated by tracing the sequences of the transmission and scattering of impulses. The theory and the demonstrated examples are presented in Refs. [9–11], in which the analogy is used for between the field and the connected acoustic tubes. The extension to the elastic field is found in Refs. [12,13]. Satou et al. proposed an equivalent circuit model in time domain for the piezoelectric vibration based on the d'Alembert's principle [14]. The present work is to demonstrate the application to the sound absorbing materials. A sound-absorbing layer was considered to be simply resistive and the case when layer was placed on the room wall was examined [15]. The present work is concerned with the modeling of a lossy field for the characterization of more general sound absorbing materials. A lossy component with variable propagation velocity is introduced for sound absorbing to facilitate the energy consumption and frequency dependence. The absorption coefficient is considered for the normal, oblique and random incidence. The numerical demonstrations show that the present approach is capable of modeling the sound absorbing characteristics in homogeneous materials.

Consider a plane sound wave normally incident from air to the sound absorbing medium at $x = 0$ as illustrated in Fig. 1. The propagation speed of sound is c_1 in the air and c_2 in the absorbing medium, and the density ρ_1 and ρ_2. The incident sound striking the absorbing boundary is partly transmitted, and partly reflected. Their pressure amplitudes are defined by p_i, p_t and p_r. The pressure reflection coefficient R between the two media is the ratio of the reflected to the incident defined by $R = p_r/p_i$. The amount of energy going into the transmission and the reflection depends on the absorbing medium's acoustic properties, from which the absorption coefficient is characterized. The absorption coefficient is defined by the ratio of the absorbed energy to the incident energy so that $\alpha = 1 - |R|^2 = 1 - p_r^2/p_i^2$. Absorption coefficient depends on the frequency so that $\alpha(f) = 1 - |P_r(f)|^2/|P_i(f)|^2$. The temporal responses $p_i(t)$ and $p_r(t)$ are Fourier-transformed into the frequency domain $P_i(f)$ and $P_r(f)$. With the lumped constant models and the one-dimensional (1D) modeling, the electrical equivalent circuit model and the electrical transmission line equivalence have for many years been used by the electro-acoustical engineers for the electro-acoustical device design in frequency domain. The time-domain approach in the transmission-line matrix (TLM) modeling is attempted to extend into 2D cases. The TLM method is equivalent to the Huygens' principle in which the physical process of the wave propagation is simulated as the sequences of the impulse transmission and scattering. When the frequency characteristic is required, its Fourier transform provides a full wave analysis.

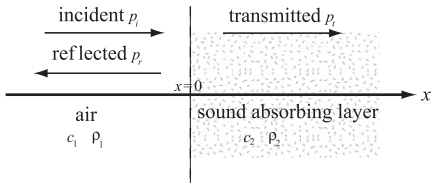

Fig. 1. Normally incident wave to a sound-absorbing layer.

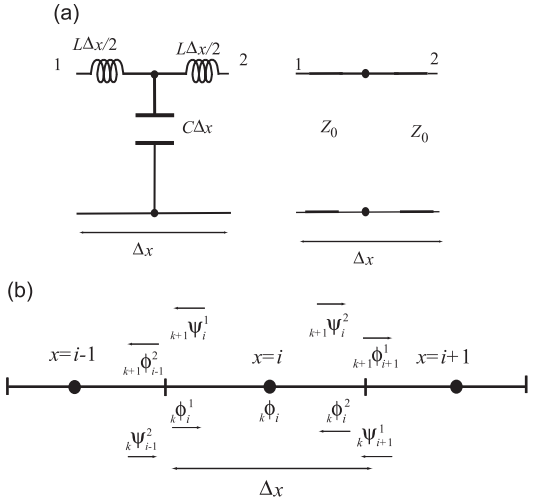

Fig. 2. One-dimensional field model: (a) a single section—the lumped model and the transmission-line model and (b) elements in series connection.

2. Wave propagation in the 1D TLM model

2.1. 1D TLM element—scattering matrix and wave equation [12]

Plane wave propagation is expressed in terms of the 1D field model which is equivalent to the electrical transmission line.

Distributed element and its lumped circuit element with two ports are depicted in Fig. 2a. L and C are the equivalent inductance and capacitance for a unit length. One section of the line or TLM element consists of two branches whose characteristic impedance is defined by $Z_0 = \sqrt{L/C}$ and propagation velocity $c = 1/\sqrt{LC}$. The homogeneous sound field is modeled by a series of the TLM elements as shown in Fig. 2b. ϕ and ψ are the velocity potentials for the input impulses and the output impulses to the node placed at an element center, respectively. For node i of the element, the input impulses are ${}_k\phi_i^1$ and ${}_k\phi_i^2$ at time $t = k\Delta t$, and the output (transmitted and reflected) impulses are ${}_{k+1}\psi_i^1$ and ${}_{k+1}\psi_i^2$ at time $t = (k+1)\Delta t$ with the time delay of Δt, where k is the integer number and the superscript indicates the port number.

The relations for this sequence are given by

$$ {}_{k+1}\begin{bmatrix} \psi_i^1 \\ \psi_i^2 \end{bmatrix} = \begin{bmatrix} 0 & 1 \\ 1 & 0 \end{bmatrix}_k \begin{bmatrix} \phi_i^1 \\ \phi_i^2 \end{bmatrix}. \tag{1} $$

So that the velocity potential at i is

$$ {}_k\phi_i = {}_k\phi_i^1 + {}_k\phi_i^2. \tag{2} $$

As the output impulses become the input impulses to the adjacent elements, the compatibility conditions for connection are

$$ {}_k\phi_{i+1}^1 = {}_k\psi_i^2, \quad {}_k\phi_{i-1}^2 = {}_k\psi_i^1. \tag{3} $$

From Eqs. (1)–(3), one obtains the expression

$$ {}_{k+1}\phi_i - 2{}_k\phi_i + {}_{k-1}\phi_i = {}_k\phi_{i+1} - 2{}_k\phi_i + {}_k\phi_{i-1}. \tag{4} $$

This is a finite difference-time domain expression, which can be expanded in Taylor series about ${}_k\phi_i$ to give the differential expression

$$\frac{\partial^2\phi}{\partial t^2}-\frac{1}{c_1^2}\frac{\partial^2\phi}{\partial x^2}+2\left\{\frac{\Delta t^2}{4!}\left(\frac{\partial^4\phi}{\partial t^4}-c_1^4\frac{\partial^4\phi}{\partial x^4}\right)+\frac{\Delta t^4}{6!}\left(\frac{\partial^6\phi}{\partial t^6}-c_1^6\frac{\partial^6\phi}{\partial x^6}\right)+\cdots\right\}=0, \tag{5}$$

where as ${}_k\phi_i$ is the velocity potential at an arbitrary point, ${}_k\phi_i$ is replaced by ϕ in Eq. (5). It corresponds to the wave equation for ϕ with higher order error terms removed as a result of the discretization, that is

$$\frac{\partial^2\phi}{\partial x^2}-\frac{1}{c_1^2}\frac{\partial^2\phi}{\partial t^2}=0, \tag{6}$$

where c_1 is the propagation speed in the transmission line $c_1=\Delta x/\Delta t$, that is also the speed in free space.

In acoustical engineering, pressure p is often used for velocity potential ϕ. The relation of p to ϕ is $p=\rho(\partial\phi/\partial t)=\rho(\Delta\phi/\Delta t)=(\phi_i-\phi_{i-1})/\Delta t$. In the followings, as we refer both quantities in relative values, they are treated as similar entity.

2.2. 1D TLM element for lossy and variable propagation velocity medium

The sound absorbing materials form a lossy field of variable propagation speed. It can be modeled by providing an additional capacitance for changing the propagation speed and a conductance for the loss. That is, the third branch or a stab of the length $\Delta l/2$ with the characteristic impedance $Z_3=Z_0/\eta$ is connected and the forth branch of infinite length with the characteristic impedance $Z_4=Z_0/\zeta$ is also connected, as illustrated in Fig. 3a. Elements are connected in series as shown in Fig. 3b to express the field. $\eta=1/(Z_3/Z_0)$ is the parameter to describe the relative admittance of the branch 3 for adjusting the propagation velocity, $\zeta=1/(Z_4/Z_0)$ is the parameter to describe the relative admittance of the branch 4 for adjusting the damping.

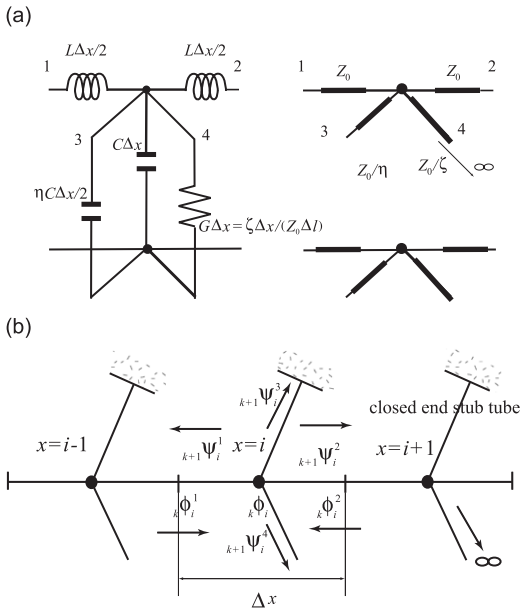

Fig. 3. One-dimensional lossy and variable propagation velocity field model: (a) a single section—the lumped model and the transmission−line model open-circuited, or a closed stub tube and (b) elements in series connection.

The scattering matrix expression [11] for the velocity potential at i are given by

$$_{k+1}\begin{bmatrix}\psi_i^1\\ \psi_i^2\\ \psi_i^3\end{bmatrix}=\frac{1}{2+\eta+\zeta}\begin{bmatrix}-\eta-\zeta & 2 & 2\eta\\ 2 & -\eta-\xi & 2\eta\\ 2 & 2 & \eta-\zeta-2\end{bmatrix}_k\begin{bmatrix}\phi_i^1\\ \phi_i^2\\ \phi_i^3\end{bmatrix}. \tag{7}$$

The impulse $_{k+1}\psi_i^4$ scattered to the forth branch is absorbed at infinity and does not go back, so that

$$_k\phi_i=\left(1-\frac{\zeta}{2+\eta+\zeta}\right)\left(\frac{2}{2+\eta}(_k\phi_i^1+{}_k\phi_i^2)+\frac{2\eta}{2+\eta}{}_k\phi_i^3\right) \tag{8}$$

or

$$_k\phi_i=\left(1-\frac{\zeta}{2+\eta+\zeta}\right)_k\phi_i',$$

where $_k\phi_i'$ is the velocity potential of lossless medium with variable propagation speed. The attenuation factor or the attenuation value per a unit length is defined as

$$\chi=\frac{\zeta}{2+\eta+\zeta}. \tag{9}$$

The reflected impulses become the input impulses to the adjacent elements so that the compatibility conditions are

$$_k\phi_{i+1}^1={}_k\psi_i^2,\quad {}_k\phi_{i-1}^2={}_k\psi_i^1. \tag{10}$$

One can obtain the expression similar to the Eq. (4)

$$(_{k+1}\phi_i-2{}_k\phi_i+{}_{k-1}\phi_i)+\frac{\zeta}{2+\eta}(_{k+1}\phi_i-{}_{k-1}\phi_i)=\frac{2}{2+\eta}(_k\phi_{i+1}-2{}_k\phi_i+{}_k\phi_{i-1}). \tag{11}$$

This is the finite difference-time domain expression, from which one has the differential expression by removing higher order error terms as

$$\frac{\partial^2\phi}{\partial x^2}-\frac{2+\eta}{2}\frac{\Delta t^2}{\Delta x^2}\frac{\partial^2\phi}{\partial t^2}+\frac{\zeta\Delta t}{\Delta x^2}\frac{\partial\phi}{\partial t}=0. \tag{12}$$

Eq. (12) can be modified to be

$$\frac{\partial^2\phi}{\partial x^2}-\frac{1}{c_2^2}\frac{\partial^2\phi}{\partial t^2}+\frac{\zeta_2}{c_2}\frac{\partial\phi}{\partial t}=0, \tag{12}'$$

where $\zeta_2=\sqrt{(2/2+\eta)}\zeta/\Delta x$ and the propagation speed $c_2=\sqrt{(2/2+\eta)}c_1$. c_1 is the propagation speed in free space.

3. Sound wave traveling into the sound-absorbing layer

3.1. The normal incidence absorption coefficient

A testing is first made for the 1D wave normally incident into a sound-absorbing layer from free space as shown in Fig. 4, where the sound speed and the density of the two media are chosen to be $c_1=340\,\mathrm{m/s}$,

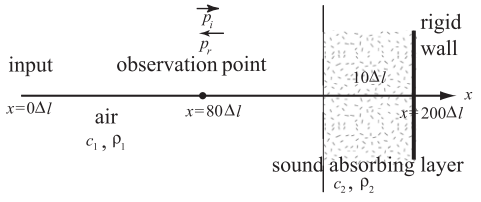

Fig. 4. Simulation of wave penetration into sound absorbing layer (one-dimensional TLM model).

$c_2 = 240\,\mathrm{m/s}$ and $\rho_1 = 1.2\,\mathrm{kg/m^3}$, $\rho_2 = 16\,\mathrm{kg/m^3}$, respectively. The attenuation factor χ in a sound-absorbing layer is chosen to be 0.01667 (this value is simply given for $\eta = 2.01398$ and $\zeta = 0.068$ in 1D TLM element and $\eta = 4.02778$ and $\zeta = 0.13609$ in 2D TLM element. These values do not refer any particular material and just chosen for convenience.) The whole field consists of $200\Delta l$ (element length $\Delta l = 0.85\,\mathrm{mm}$) in which $10\Delta l$ is allocated for the sound-absorbing layer. An impulsive sound source is emitted at the left end and the sound-absorbing layer is backed by the rigid wall. The incident and reflected waves observed at point $i = 80$ and the spectra Fourier-transformed are shown in Fig. 5.

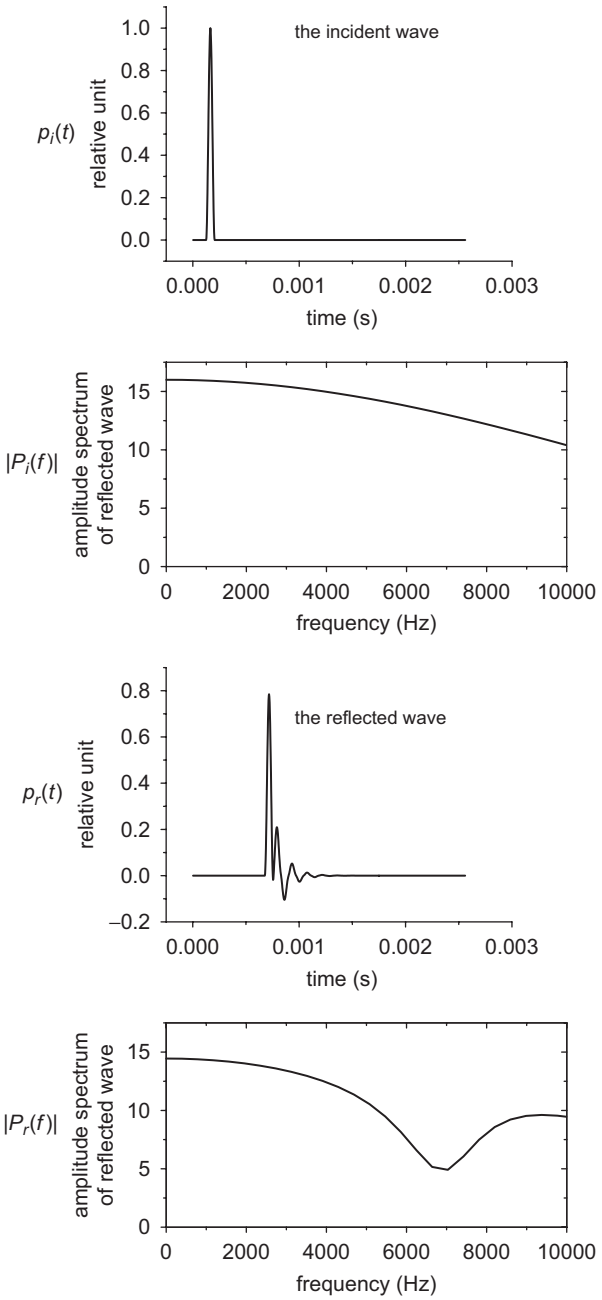

Fig. 5. The incident and reflected waves observed at point $i = 80$ and the spectra Fourier-transformed from the temporal domain to frequency domain.

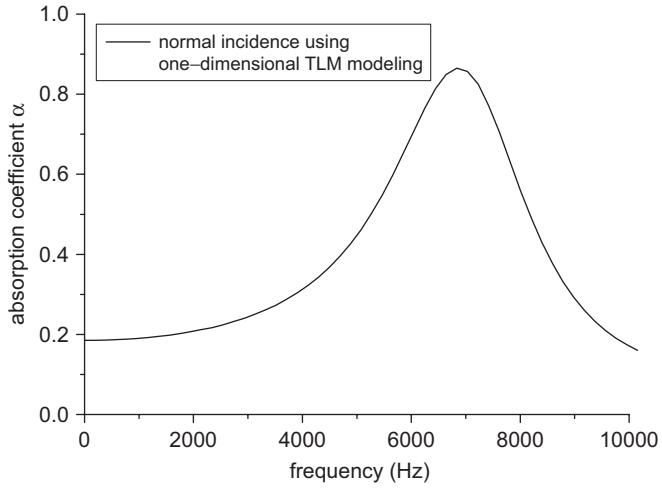

Fig. 6. The normal incidence absorption coefficient using one-dimensional TLM modeling.

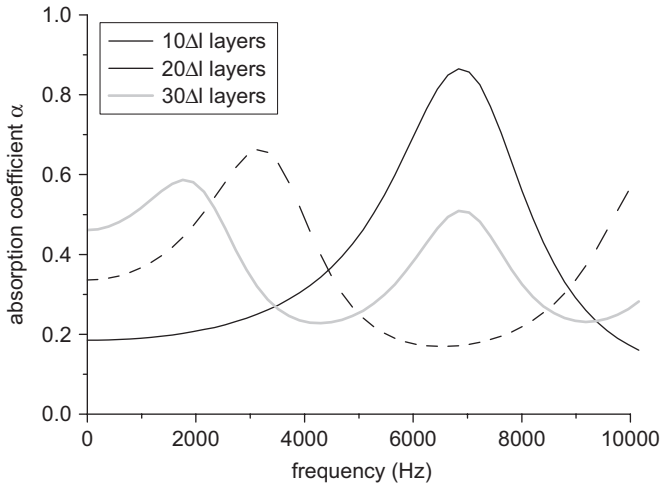

Fig. 7. Effect of absorbent thickness.

Both $P_i(f)$ and $P_r(f)$ are complex number and their magnitudes are shown in the figures. The normal incidence absorption coefficient is defined in terms of the energy ratio as

$$\alpha(f) = 1 - \frac{|P_r(f)|^2}{|P_i(f)|^2}, \tag{13}$$

which is shown in Fig. 6. The figure shows a selective characteristic due to the layer's thickness resonance.

3.1.1. The absorption characteristics

The absorption characteristics of the absorbing material are determined by many factors. The simulation shows the curves of the absorption coefficient in frequency domain in which the change of the thickness shift the resonance peak characteristics.

Fig. 7 illustrates the effect of material thickness. Each absorber is mounted on a rigid wall. As the thickness increases from $10\Delta l$ to $30\Delta l$, the frequency corresponding to half wavelength at which the absorption peaks decreases. In the thickest case, the higher second resonance appears.

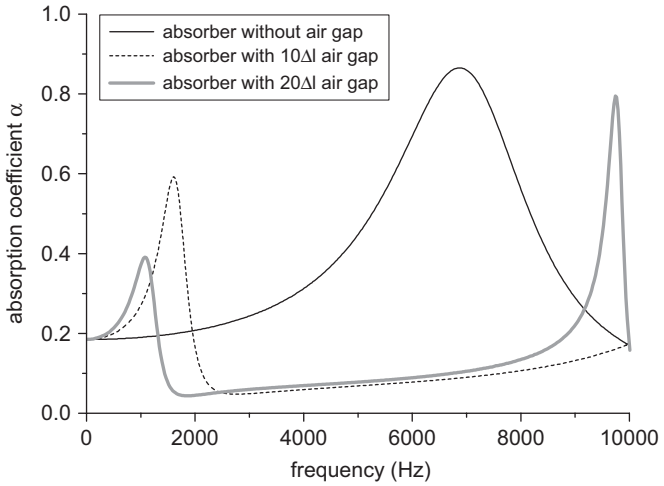

Fig. 8. Effect of air gap behind absorber.

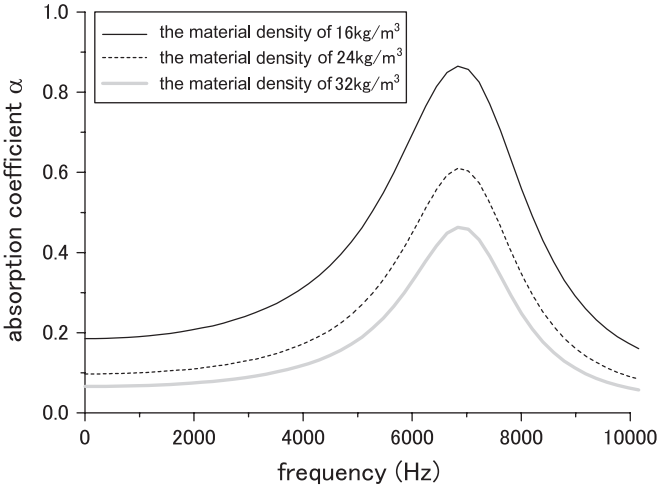

Fig. 9. Effect of material density.

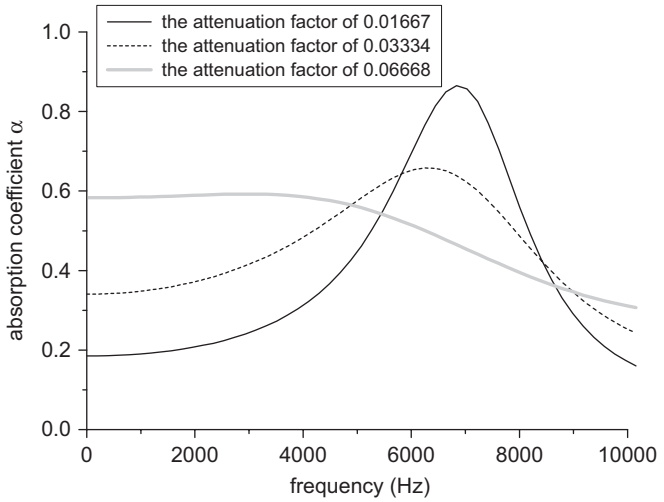

Fig. 10. Effect of material resistivity.

Fig. 8 shows the effect of an air space placed between the absorbing layer and the backing rigid wall. As the space gap increases from $0\Delta l$ to $20\Delta l$, the peak frequency moves down to lower frequency. The spacing works as to increase the effective thickness of the absorbing layer.

Fig. 9 shows the effect of the material density. As the density increases, the absorption coefficient decreases as a whole.

Fig. 10 shows the effect of the material's attenuation factor. The attenuation relates not only to the resistive component but also to the reactive component as defined by Eq. (9). As the attenuation factor increases, the absorption increases at lower frequency pushing the peak down. The attenuation factor and the propagation velocity can be measured in the experiment, from which the parameters η and ζ needed in our TLM model can be obtained.

4. Normal incident propagation on a transmission line—frequency domain solution

The transmission line theory is well established in electrical engineering in which the solution is used to be sought in frequency domain. No direct time-domain solution has been attempted except that the inverse Fourier/Laplace transform approach is used from the frequency domain solution.

A lossless transmission line model is shown in Fig. 11(a). The wave equation is given for the potential ϕ by

$$\frac{\mathrm{d}^2\phi(x)}{\mathrm{d}x^2} - LC\frac{\mathrm{d}^2\phi(x)}{\mathrm{d}t^2} = 0, \tag{14}$$

where L and C are the inductance and capacitance per unit length.

It is the same as Eq. (6), in which propagation speed is $c_1 = 1/\sqrt{LC}$.

The solution is given in the form

$$\phi(x) = \phi^+ \mathrm{e}^{-\mathrm{j}\beta x} + \phi^- \mathrm{e}^{\mathrm{j}\beta x}, \tag{15}$$

$\phi^+ \mathrm{e}^{-\mathrm{j}\beta x}$ is the wave propagating in the $+x$ direction, while $\phi^- \mathrm{e}^{\mathrm{j}\beta x}$ is the wave propagating in the reverse $-x$ direction, where $\beta = \omega\sqrt{LC}$ is the phase constant.

The characteristic impedance of the lossless line is $Z_1 = \sqrt{L_1/C_1}$.

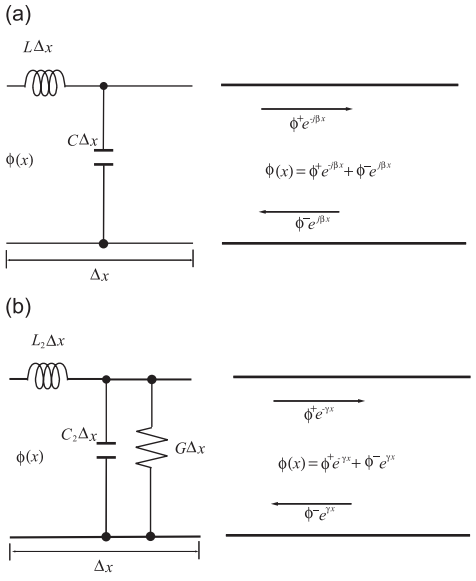

Fig. 11. A one-dimensional transmission line: (a) loss-less line and (b) lossy line.

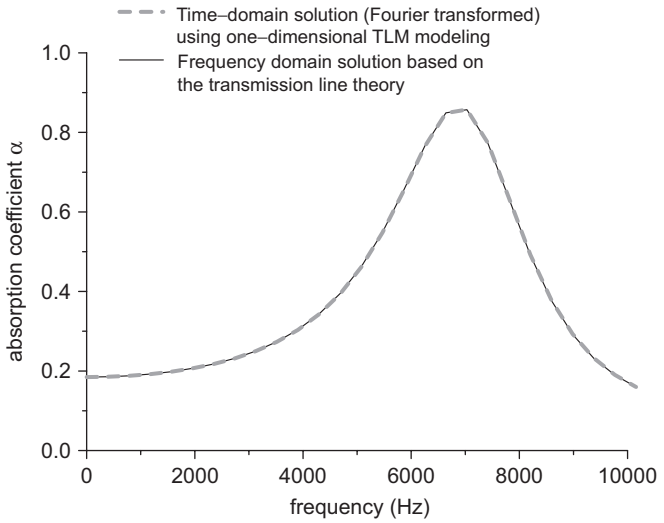

Fig. 12. An example of the normal incidence absorption coefficient calculated based on the two models.

Fig. 11(b) shows a lossy transmission line, in which the shunt conductance G is inserted. The wave equation is

$$\frac{\partial^2\phi}{\partial x^2} - L_2C_2\frac{\partial^2\phi}{\partial t^2} - GL_2\frac{\partial\phi}{\partial t} = 0, \tag{16}$$

where L_2 and C_2 are the inductance and the capacitance per unit length.

It is the same as Eq. (12)′ but for the propagation speed $c_2 = 1/\sqrt{L_2C_2}$ and the shunt conductance $G = \zeta_2/\sqrt{L_2/C_2} = \zeta_2/Z_2'$, where $Z_2' = \sqrt{L_2/C_2}$ is the characteristic impedance of the transmission line.

The solution for $\phi(x)$ is given in the form

$$\phi(x) = \phi^+ e^{-\gamma x} + V^- e^{\gamma x}, \tag{17}$$

where $\gamma = j\beta + \alpha = \sqrt{j\omega L_2(j\omega C_2 + G)}$. α is the attenuation constant. Please note that α is different from previous definition of sound absorption coefficient.

The characteristic impedance of the lossy media is $Z_2 = \sqrt{j\omega L_1/(j\omega C_1 + G)}$.

By comparing Eqs. (6) and (14) with Eqs. (12)′ and (16), one can establish the relation $L = \rho_1$, $C = 1/(\rho_1 c_1^2)$ and $L_2 = \rho_2$, $C_2 = 1/(\rho_2 c_2^2)$, and $G = \zeta_2/Z_2' = \sqrt{(2/(2+\eta))\zeta/(Z_2'\Delta l)}$.

At the interface between the two media, the reflection coefficient is given by the relationship as

$$R = \frac{Z_2 - Z_1}{Z_2 - Z_1} = \frac{\sqrt{j\omega L_2/(j\omega C_2 + G)} - \sqrt{j\omega L/j\omega C}}{\sqrt{j\omega L_2/(j\omega C_2 + G)} + \sqrt{j\omega L/j\omega C}}. \tag{18}$$

The transmission coefficient is therefore

$$T = 1 - R. \tag{19}$$

The matrix expression for the incident and reflected waves are given [16] as

$$\begin{bmatrix} P_i(f) \\ P_r(f) \end{bmatrix} = \frac{1}{T}\begin{bmatrix} 1 & R \\ R & 1 \end{bmatrix}\begin{bmatrix} e^{\gamma x} & 0 \\ 0 & e^{-\gamma x} \end{bmatrix}\begin{bmatrix} P_{ie} \\ P_{re} \end{bmatrix}, \tag{20}$$

where P_e is the pressure at the right-hand side end of the layer.

When the end boundary condition is rigid there, the incident and the reflected are the same so that

$$P_{ie} = P_{re}. \tag{21}$$

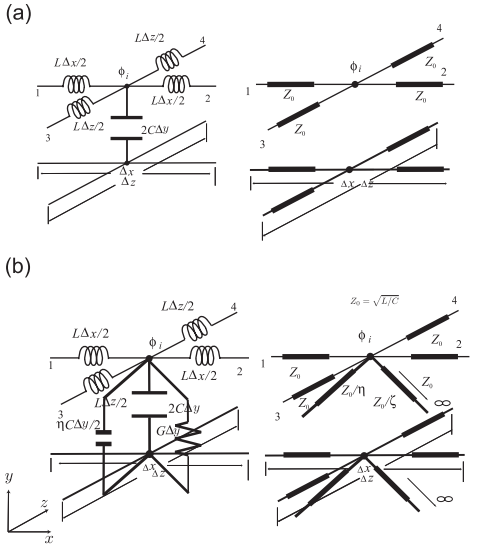

Fig. 13. Two-dimensional TLM models $\left(Z_0 = \sqrt{L/C}\right)$: (a) lossless and (b) lossy.

Comparison is made for the normal incidence absorption coefficients in two models, which are shown in Fig. 12. Both methods give the same result and thus the present time domain method using TLM is justifiable.

5. 2D model for oblique incidence

The absorption coefficient of the absorbing materials is known depending on the angle of the incidence. Here, a 2D TLM model is considered. The lumped circuit element and the distributed element for free space are depicted in Fig. 13(a). L and C are the equivalent inductance and capacitance for the unit length. Appling the Kirchhoff's voltage and current laws on the circuit element, the differential expression about (velocity) potential ϕ is derived as

$$\frac{\partial^2\phi}{\partial x^2} + \frac{\partial^2\phi}{\partial z^2} = \frac{1}{c^2}\frac{\partial^2\phi}{\partial t^2}, \tag{22}$$

where $c = c_1/\sqrt{2}$. It should be noted that the propagation speed in the 2D network is slower than that in free space by the factor $\sqrt{2}$.

The scattering matrix expression for the coming and scattering impulses is given by

$$_{k+1}\begin{bmatrix}\psi^1_{x,z}\\ \psi^2_{x,z}\\ \psi^3_{x,z}\\ \psi^4_{x,z}\end{bmatrix} = \frac{1}{2}\begin{bmatrix}-1 & 1 & 1 & 1\\ 1 & -1 & 1 & 1\\ 1 & 1 & -1 & 1\\ 1 & 1 & 1 & -1\end{bmatrix}_k \begin{bmatrix}\phi^1_{x,z}\\ \phi^2_{x,z}\\ \phi^3_{x,z}\\ \phi^4_{x,z}\end{bmatrix}, \tag{23}$$

in which $_k\phi^n_{x,z}(n = 1\sim4)$ is the input impulse on the branch n at time $t = k\Delta t$ and $_{k+1}\psi^n_{x,z}$ refers to the scattered one at the next time step. The potential at node x, z is evaluated to be

$$_k\phi_{x,z} = \left\{{}_k\phi^1_{x,z} + {}_k\phi^2_{x,z} + {}_k\phi^3_{x,z} + {}_k\phi^4_{x,z}\right\}\Big/2. \tag{24}$$

As the output impulses from an element become the input impulses to the adjacent elements, the compatibility conditions for connection are

$$_k\phi^1_{x+1,z} = {}_k\psi^2_{x,z}, \quad {}_k\phi^2_{x-1,z} = {}_k\psi^1_{x,z}, \quad {}_k\phi^3_{x,z+1} = {}_k\psi^4_{x,z}, \quad {}_k\phi^4_{x,z-1} = {}_k\psi^3_{x,z}. \tag{25}$$

From Eqs. (23)–(25), one obtains the expression

$$2({}_{k+1}\phi_{x,y} - 2{}_{k}\phi_{x,y} + {}_{k-1}\phi_{x,y}) = {}_{k}\phi_{x-1,z} + {}_{k}\phi_{x+1,z} + {}_{k}\phi_{x,z-1} + {}_{k}\phi_{x,z+1} - 4{}_{k}\phi_{i}. \tag{26}$$

This is a finite difference-time domain expression, which can be expanded in Taylor series about ${}_{k}\phi_{i}$ as before to give the differential expression

$$\frac{\partial^2\phi}{\partial x^2} + \frac{\partial^2\phi}{\partial z^2} - \frac{2\Delta t^2}{\Delta l^2}\frac{\partial^2\phi}{\partial t^2} + \frac{2}{\Delta l^2}\left\{\frac{\Delta l^2}{4!}\left(\frac{\partial^4\phi}{\partial x^4} + \frac{\partial^4\phi}{\partial z^4}\right) + \frac{\Delta l^6}{6!}\left(\frac{\partial^6\phi}{\partial x^6} + \frac{\partial^6\phi}{\partial z^6}\right) + \cdots\right\} - \frac{4}{\Delta l^2}\left\{\frac{\Delta t^4}{4!}\frac{\partial^4\phi}{\partial t^4} + \frac{\Delta t^6}{6!}\frac{\partial^6\phi}{\partial t^6} + \cdots\right\} = 0. \tag{27}$$

Eq. (27) corresponds to the wave equation for ϕ with higher order error terms removed as a result of the discretization, that is

$$\frac{\partial^2\phi}{\partial x^2} + \frac{\partial^2\phi}{\partial z^2} - \frac{1}{c^2}\frac{\partial^2\phi}{\partial t^2} = 0, \tag{28}$$

where the propagation speed is $c = \Delta l/(\sqrt{2}\Delta t) = c_1/\sqrt{2}$. c_1 is the propagation speed in free space.

A lossy TLM element for the sound-absorbing field is obtained by increasing the capacitance with the addition of an open stub or a closed end stub tube for adjusting the propagation speed and by introducing the conductance for the loss, which is shown in Fig. 13(b). The scattering matrix expression is given as

$$\begin{matrix}{}_{k+1}\end{matrix}\begin{bmatrix}\psi^1_{x,z}\\ \psi^2_{x,z}\\ \psi^3_{x,z}\\ \psi^4_{x,z}\\ \psi^5_{x,z}\end{bmatrix} = \frac{1}{4+\eta+\zeta}\begin{bmatrix}-2-\eta-\zeta & 1 & 1 & 1 & \eta\\ 1 & -2-\eta-\zeta & 1 & 1 & \eta\\ 1 & 1 & -2-\eta-\zeta & 1 & \eta\\ 1 & 1 & 1 & -2-\eta-\zeta & \eta\\ 1 & 1 & 1 & 1 & \eta-\zeta-4\end{bmatrix}_{k}\begin{bmatrix}\phi^1_{x,z}\\ \phi^2_{x,z}\\ \phi^3_{x,z}\\ \phi^4_{x,z}\\ \phi^5_{x,z}\end{bmatrix} \tag{29}$$

and the nodal potential at the element center is

$${}_{k}\phi_{x,z} = \left(1 - \frac{\zeta}{4+\eta+\zeta}\right)\left[\frac{2}{4+\eta}\left({}_{k}\phi^1_{x,z} + {}_{k}\phi^2_{x,z} + {}_{k}\phi^3_{x,z} + {}_{k}\phi^4_{x,z}\right) + \frac{2\eta}{4+\eta}{}_{k}\phi^5_{x,z}\right]. \tag{30}$$

The attenuation factor is the attenuation per unit element length, which is

$$\chi = \frac{\zeta}{4+\eta+\zeta}. \tag{31}$$

As the output impulses become the input impulses to the adjacent elements, the compatibility conditions for connection are

$${}_{k}\phi^1_{x+1,z} = {}_{k}\psi^2_{x,z}, \quad {}_{k}\phi^2_{x-1,z} = {}_{k}\psi^1_{x,z}, \quad {}_{k}\phi^3_{x,z+1} = {}_{k}\psi^4_{x,z}, \quad {}_{k}\phi^4_{x,z-1} = {}_{k}\psi^3_{x,z} \tag{32}$$

one obtains the expression similar to Eq. (11)

$$\left({}_{k+1}\phi_{x,y} - 2{}_{k}\phi_{x,y} + {}_{k-1}\phi_{x,y}\right) + \frac{\zeta}{4+\eta}\left({}_{k+1}\phi_{x,y} - {}_{k-1}\phi_{x,y}\right) = \frac{2}{4+\eta}\left({}_{k}\phi_{x-1,z} + {}_{k}\phi_{x+1,z} + {}_{k}\phi_{x,z-1} + {}_{k}\phi_{x,z+1} - 4{}_{k}\phi_{i}\right). \tag{33}$$

This is the finite difference-time domain expression, form which one has the differential expression by removing higher order error terms

$$\frac{\partial^2\phi}{\partial x^2} + \frac{\partial^2\phi}{\partial z^2} - \frac{4+\eta}{2}\frac{\Delta t^2}{\Delta l^2}\frac{\partial^2\phi}{\partial t^2} + \frac{\zeta\,\Delta t}{\Delta l^2}\frac{\partial\phi}{\partial t} = 0. \tag{34}$$

Eq. (34) can be modified to be

$$\frac{\partial^2\phi}{\partial x^2} + \frac{\partial^2\phi}{\partial z^2} - \frac{1}{c_T^2}\frac{\partial^2\phi}{\partial t^2} - \frac{\zeta_T}{c_T}\frac{\partial\phi}{\partial t} = 0, \tag{34}'$$

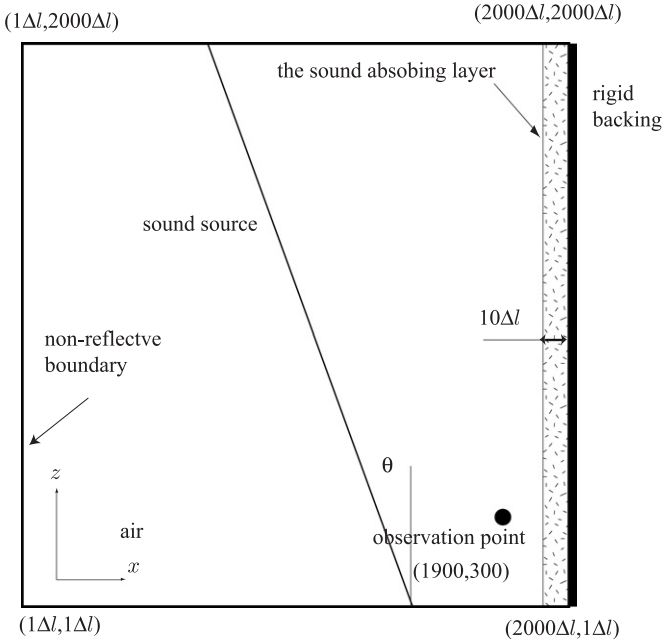

Fig. 14. Simulation field for oblique incidence.

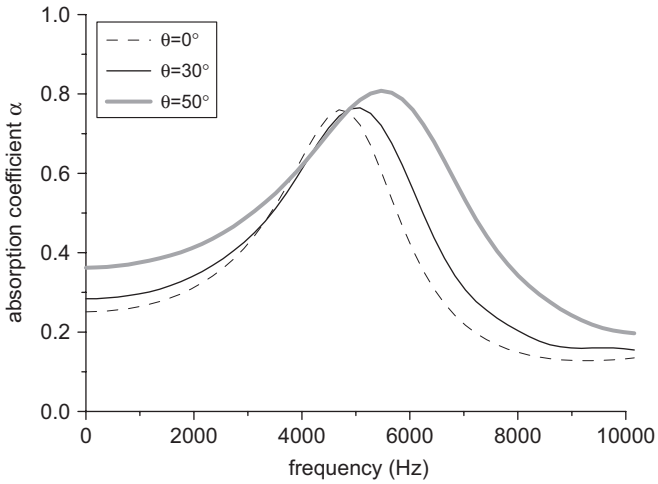

Fig. 15. The absorption coefficient for different angles of incidence in two-dimensional TLM model.

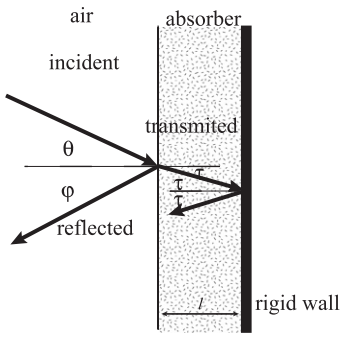

Fig. 16. Geometry for propagation of sound through a finite layer absorber with a rigid wall backed.

where the propagation speed is $c_T = \sqrt{(2/(4+\eta))}c_1$ and $\zeta_T = \sqrt{(2/(4+\eta))}\zeta/\Delta l$. c_1 is the propagation speed in free space.

Consider a sound wave incident to the surface of the sound-absorbing layer surface at an angle θ. The layer is again assumed to be backed by the rigid wall. The geometry of the simulation field is shown in Fig. 14.

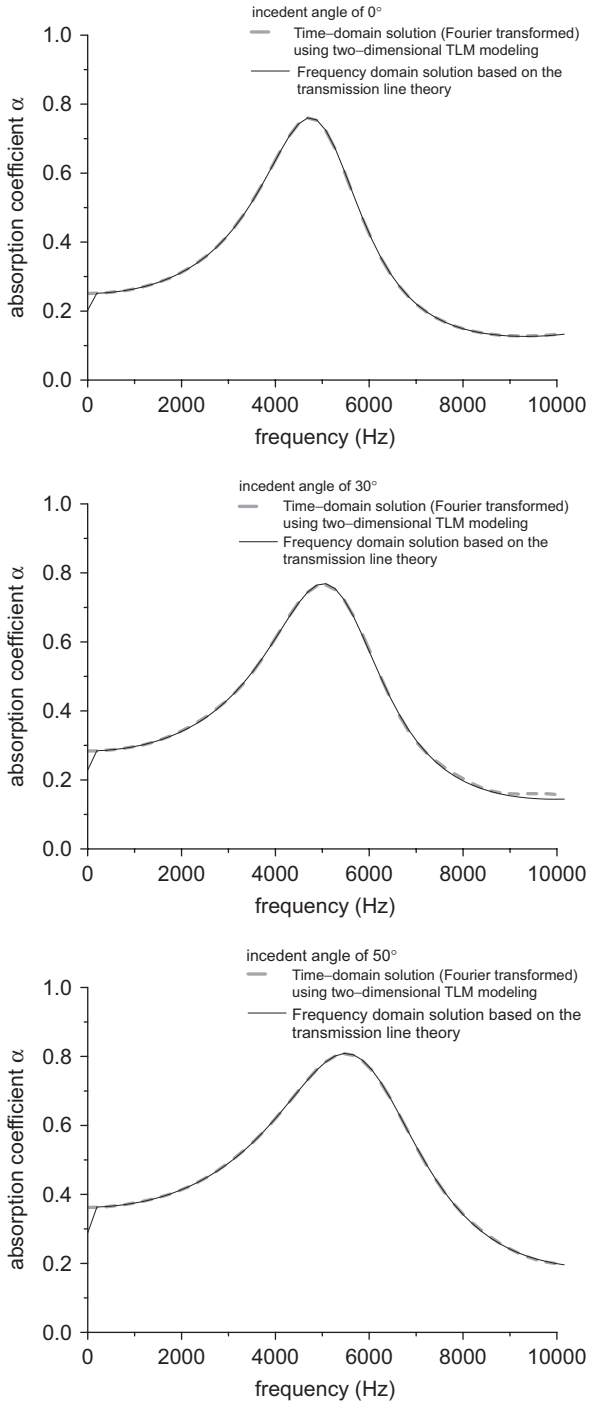

Fig. 17. Comparison of absorption coefficient characteristics, two kinds of solution of TLM modeling and transmission line theory at different angles of incidence.

The sound speed and the martial density are $c_1 = 340\,\mathrm{m/s}$, $\rho_1 = 1.2\,\mathrm{kg/m^3}$ for air, and for the sound-absorbing layer, they are $c_2 = 240\,\mathrm{m/s}$, $\rho_2 = 16\,\mathrm{kg/m^3}$. The attenuation coefficient χ of the sound-absorbing layer is again chosen to be 0.01667. The whole field consists of $2000\Delta l \times 2000\Delta l$ mesh ($\Delta l = 0.85\,\mathrm{mm}$), the surrounding of which has the non-reflective characteristic impedance termination. The sound-absorbing layer has $10\Delta l$ thickness. The incident and reflected waves are observed at the observation point marked in the figure. From these waveforms, the absorption coefficient is calculated for the different angles of incidence. This arrangement simulates the experimental setup for the absorption coefficient measurement on the site for the various incidence angles. Some results are shown in Fig. 15.

For the normal incidence, if the frequency measure is scaled up by the factor $\sqrt{2}$, it gives the similar characteristic to that of the 1D model. As the incident angle increases, the peak of the absorption characteristic shifts upwards in frequency.

6. Oblique incident propagation on the 1D transmission line model—geometrical consideration

Consider a plane sound wave incident at an angle θ to a homogenous absorbing layer of finite thickness with a rigid backing. The wave is reflected at angle $\varphi(\varphi = \theta)$ at the air-absorber interface and the some transmits into absorber at angle τ. The geometry is shown in Fig. 16. The wavenumber in air is k_1, and the wavenumber in the absorber is k_2. Snell's law implies the relation between the angles and the wavenumbers to be

$$k_1 \sin\theta = k_2 \sin\tau. \tag{35}$$

The wavenumber is inversely related to the wavelength $k = 2\pi/\lambda$ and corresponds to the phase constant mentioned in Section 4. The wavenumber in air is $k_1 = \beta = \omega\sqrt{LC}$, and the wavenumber in the absorber is a complex number $k_2 = \sqrt{\omega^2 L_2 C_2 - \mathrm{j}\omega L_2 G} = \mathrm{j}\gamma$ where γ is the propagation constant $\gamma = \sqrt{-\omega^2 L_2 C_2 + \mathrm{j}\omega L_2 G}$.

With the transmission line theory, in the case of oblique incidence, the equivalent characteristic impedance and the propagation constant depend on the angle of incidence and transmission [17]. Characteristic impedance depends on $1/\cos\theta$, the propagation constant is varied with $\cos\theta$.

The reflection coefficient for the oblique incidence is therefore given by

$$R = \frac{Z_2/\cos\tau - Z_1/\cos\theta}{Z_2/\cos\tau - Z_1/\cos\theta} = \frac{\sqrt{\mathrm{j}\omega L_2/(\mathrm{j}\omega C_2 + G)}/\cos\tau - \sqrt{\mathrm{j}\omega L/\mathrm{j}\omega C}/\cos\theta}{\sqrt{\mathrm{j}\omega L_2/(\mathrm{j}\omega C_2 + G)}/\cos\tau + \sqrt{\mathrm{j}\omega L/\mathrm{j}\omega C}/\cos\theta} \tag{36}$$

and the transmission coefficient is

$$T = 1 - R. \tag{37}$$

The matrix expression for the incident and reflected waves is given as

$$\begin{bmatrix} P_i(\theta) \\ P_r(\theta) \end{bmatrix} = \frac{1}{T}\begin{bmatrix} 1 & R \\ R & 1 \end{bmatrix}\begin{bmatrix} \mathrm{e}^{-\mathrm{j}k_2 l\cos\tau} & 0 \\ 0 & \mathrm{e}^{-\mathrm{j}k_2 l\cos\tau} \end{bmatrix}\begin{bmatrix} P_{ie} \\ P_{re} \end{bmatrix}, \tag{38}$$

where P_i and P_r refer to the coming and reflected pressure at the input and P_{ie} and P_{re} refer to the pressure at the output end of the layer. The layer is modeled as a four terminals transmission line. As the end boundary condition is rigid there, the incident and the reflected are the same so that

$$P_{ie} = P_{re}. \tag{39}$$

The absorption coefficient is given by

$$\alpha(\theta) = 1 - \frac{|P_r(\theta)|^2}{|P_i(\theta)|^2}.$$

The comparison is made for the oblique incidence absorption coefficient between the 1D transmission-line theory and the simulated result for the 2D TLM model as shown in Fig. 17. The two solutions give exactly the same result, which again validates our TLM modeling. The frequency domain analysis fails in the vicinity of zero frequency.

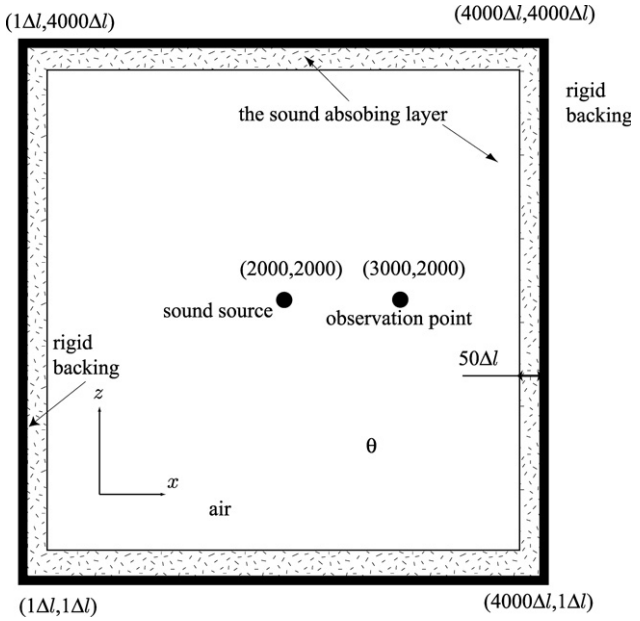

Fig. 18. The simulation model for the two-dimensional reverberation chamber.

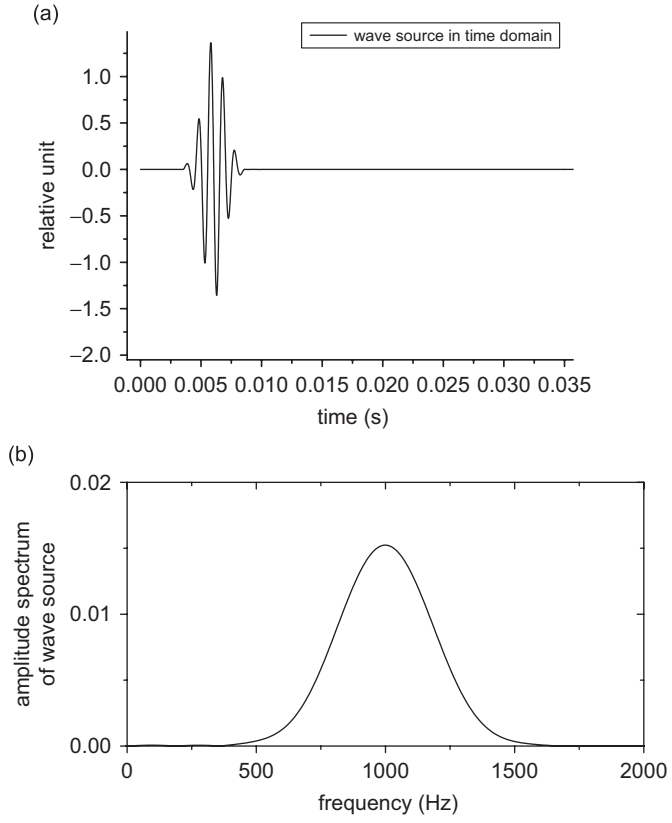

Fig. 19. The sound source in time domain and frequency domain: (a) the wave form of sound source of 1000 Hz center frequency and (b) the frequency spectra of sound source of 1000 Hz center frequency.

7. Reverberation chamber absorption coefficient—random incidence

We have discussed the absorption for the normal incidence and the oblique incidence. But in actual situation, when walls in a room are treated by the absorbers, the sound would be incident to the absorbing wall from every direction or a multitude of incident angles at once, then the evaluation for the random incidence is important.

The random incident absorption coefficient can be defined for homogenous absorbing materials by

$$\alpha_{\mathrm{ran}} = \frac{\int_0^{\pi/2} \alpha(\theta) \sin\,\theta\,\cos\,\theta\,\mathrm{d}\theta}{\int_0^{\pi/2} \sin\,\theta\,\cos\,\theta\,\mathrm{d}\theta}, \tag{40}$$

where $\alpha(\theta)$ is the absorption coefficient for the incident angle θ [18].

For more realistic applications, the reverberation chamber method is used for the averaged incident angle in which the absorption coefficient is obtained from the reverberation time measured in the reverberation chamber where the absorber is placed.

A 2D reverberation chamber is here modeled by the 2D TLM space. The chamber walls treated by the absorbing layer under test. An impulsive sound is generated at a point in the middle of the chamber.

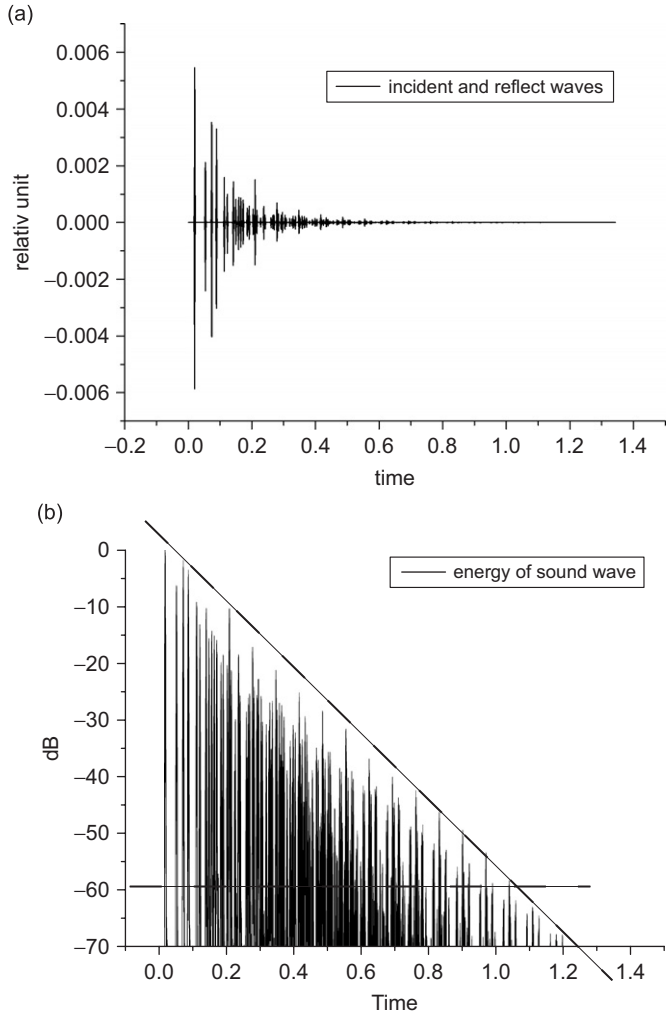

Fig. 20. The decay of the sound pressure: (a) waves form recorded at the observation point for a single shot sine wave of the 1000 Hz and (b) the pressure decay.

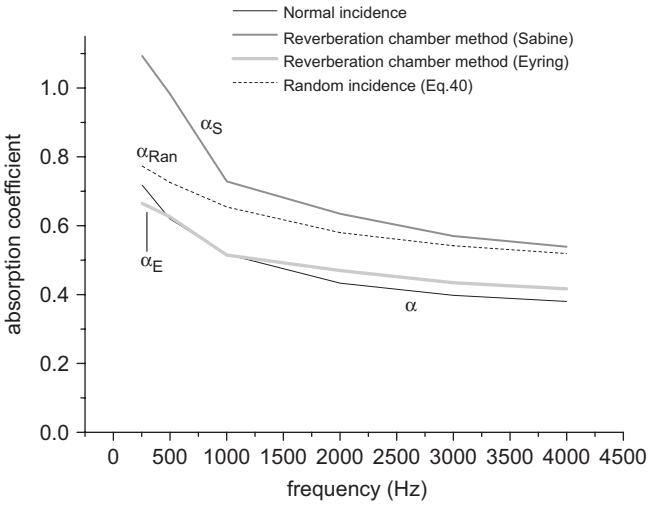

Fig. 21. Comparison of the absorption coefficient for normal and random incidences and those based on the reverberation chamber method (Sabine's and Eyring's).

The impulsive sound waves strike the walls, which are reflected repeatedly between the walls, through which the waves decay as the sound energy is absorbed. The sound pressure is recorded at a point inside the chamber and the rate of sound energy decay is measured. From this curve, the absorption coefficient of the absorber is determined. The time taken for the sound pressure level to decay by -60 dB is called the reverberation time. The Sabine's formulation or Eyring's formulation describes the relation of the reverberation time to the absorption coefficient.

The reverberation time is given for a 2D field by

$$T = \frac{6\pi S}{\bar{\alpha} D c \log_{10} e} \quad \text{Sabine's formula,} \tag{41a}$$

$$T = \frac{-6\pi S}{D c \ln(1-\bar{\alpha}) \log_{10} e} \quad \text{Eyring's formula,} \tag{41b}$$

where T is the reverberation time in seconds, c is the propagation speed of sound in air (in the present model in 2D TLM space), S is the area of the chamber, as sound wave is assumed to be absorbed only by the absorber. $\bar{\alpha}$ is the absorber's averaged absorption coefficient and D is the total surface length of the absorber.

The absorption coefficient of reverberation chamber method can be calculated by solving Eqs. (41a) or (41b) for $\bar{\alpha}$. That is

$$\bar{\alpha} = \frac{6\pi S}{DLc \log_{10} e} \quad \text{Absorption coefficient based on Sabine's formula,} \tag{41a}'$$

$$\bar{\alpha} = 1 - \mathrm{e}^{(6\pi S/DLc \log_{10} e)} \quad \text{Absorption coefficient based on Eyring's formula.} \tag{41b}'$$

These formulas are the 2D counterparts to the well-known 3D formula [3].

A simulation is made for measuring the absorption coefficient by the reverberation chamber method as shown in Fig. 18, where the whole field consists of $4000\Delta l \times 4000\Delta l$ ($\Delta l = 4.25$ mm, element length) in which the absorber of thickness $l = 50\Delta l$ is mounted on the rigid walls. The sound speed and the density of air and the absorber are chosen to be $c_1 = 340$ m/s, $c_2 = 240$ m/s and $\rho_1 = 1.2\,\mathrm{kg/m^3}$, $\rho_2 = 16\,\mathrm{kg/m^3}$ respectively. The attenuation factor χ in the absorber is chosen to be much larger value of 0.1667 per element length. Sound source of a single shot sine wave are chosen, whose central frequencies are 250, 500, 1000, 2000, 3000 and 4000 Hz. The sound is emitted at the point in the middle of the chamber. The sound source with 1000 Hz central frequency and the corresponding frequency spectra are shown in Fig. 19. The incident and reflected

waves are recorded at the observation point (3000, 2000) marked in the figure. The waveform in reverberation is shown in Fig. 20. From the pressure decay, the reverberation time is 1.08 s. The absorption coefficients are calculated based on Sabing's or Eyring's formulation. Fig. 21 shows the frequency characteristics of the absorption coefficients due to the two definitions. It is well known that Sabine's absorption coefficient is not accurate for the case of large absorption coefficient and in that range Eyring's absorption coefficient is supposed to be better. The difference of the coefficients between Sabing's and Eying's is as much as twenty percents. The absorption coefficient of the normal incidence and that of the random incidence based on Eq. (40) are also shown in the figure. The frequency characteristic does not exhibit the resonance as the attenuation factor is chosen to be much larger.

8. Concluding remarks

We proposed a lossy transmission-line matrix (TLM) model with variable propagation speed to characterize the sound-absorbing media for which the relation of the attenuation factor to the parameters in TLM models was established. The treatment simulates the direct time-domain response for absorbing materials possible. The examination was made for the frequency characteristics with the Fourier transformed for the normal and oblique incidence. The solutions were compared with the frequency domain solution based on the 1D transmission-line theory. Good agreement proved the validity of the present modeling. The simulation was extended to the case of the modeling of the reverberation chamber. In the present simulation, we are only confining ourselves to the 2D field models. It is however straightforward to extend to the 3D field modeling, as the sound is scalar, except that the 3D simulation requires more memory and computational time resources. In the extreme case of the perfect absorption, the modeling leads to the transparent boundary, which is useful for simulating an unbounded non-reflective space [19].

References

[1] H.F. Olson, *Acoustical Engineering*, D Van Nostrand, Amsterdam, 1957.
[2] H.J. Pian, *The Physics of Vibrations and Waves*, second ed., Wiley, New York, 1976.
[3] S. Kimura, *Architectural Acoustics and Noise Control Plan*, Shokokusha Publishing Co. Ltd, 1977 (in Japanese).
[4] Y. Kagawa, *Finite Elements for Acoustical Engineering*, Baifukan, Tokyo, 1981 (in Japanese).
[5] A. Craggs, A finite element model for rigid porous absorbing materials, *Journal of Sound and Vibration* 61 (1) (1978) 101–111.
[6] A. Craggs, Coupling of finite element acoustical absorption models, *Journal of Sound and Vibration* 66 (4) (1979) 605–613.
[7] Y. Kagawa, T. Yamabuchi, Finite-element equivalent circuits for acoustic field, *Journal of the Acoustical Society of America* 64 (4) (1978) 1196–1200.
[8] C. Christopoulos, *The Transmission-Line Modeling Method TLM*, IEEE Press, New York, 1995.
[9] Y. Kagawa, T. Tsuchiya, B. Fujii, K. Fujioka, 'Discrete Huygens' model approach to sound wave propagation, *Journal of Sound and Vibration* 218 (3) (1998) 419–444.
[10] Y. Kagawa, T. Tsuchiya, K. Fujioka, M. Takeuchi, 'Discrete Huygens' model approach to sound wave propagation—reverberation in a room, sound source identification and tomography in time reversal, *Journal of Sound and Vibration* 225 (1) (1999) 61–78.
[11] Y. Kagawa, T. Tsuchiya, T. Hara, T. Tuji, 'Discrete Huygens' modelling simulation of sound wave propagation in velocity varying environments, *Journal of Sound and Vibration* 246 (3) (2001) 419–439.
[12] Y. Kagawa, T. Fujitani, Y. Fujita, L. Chai, N. Wakatsuki, T. Tsuchiya, 'Discrete Huygens' modeling approach to wave propagations in a homogeneous elastic field, *Journal of Sound and Vibration* 255 (2) (2002) 323–335.
[13] P. Langley, S.H. Pulko, J. Wilkinson, A TLM model of transient, 2-dimensional stress propagation, *International Journal of Numerical Modelling: Electronic Networks, Devices and Fields* 9 (1996) 424–429.
[14] Y. Kagawa, K. Yoshida, T. Tsuchiya, M. Satou, *Introduction to Equivalent Circuit Analogy Methods*, Morikita-shuppan, Tokyo, 2000 (in Japanese).
[15] M. Takeuchi, Y. Kagawa, T. Tsuchiya, Simulation of sound wave behavior in a room by TLM modeling—sound absorbing materials, *Proceeding of the 18th Computational Electronics and Electromagnetism symposium, JSST* 2-II-4, Nov. 27–28, 1997, pp. 213–216.
[16] O. Hashimoto, *The Story of the Wave Absorber*, Nikkan Industrial News Publishing Co. Ltd., 2001 (in Japanese).
[17] K. Kagoshima, *Fundamentals and Practice in Electromagnetic Waves*, Corona Publishing Co. Ltd, 2003 (in Japanese).
[18] T.J. Cox, P. D'Antonio, *Acoustic Absorbers and Diffusers—Theory, Design and Application*, Spon Press, 2004.
[19] L. Chai, S. Nogi, Y. Kagawa, N. Wakatsuki, Absorbing boundary conditions in transmission-line matrix (TLM) modeling, *Journal of the Japan Society for Simulation Technology-Simulation* 24 (1) (2005) 59–65.